JOURNAL OF PETROLOGY | VOLUME 42 | NUMBER 1 | PAGES 89–101 | 2001

The Zircon-Bearing Chromitites of the Phlogopite Peridotite of Finero (Ivrea Zone, Southern Alps): Evidence and Geochronology of a Metasomatized Mantle Slab

G. GRIECO[1]*, A. FERRARIO[1], A. VON QUADT[2], V. KOEPPEL[2] AND E. A. MATHEZ[3]

[1]DIPARTIMENTO DI SCIENZE DELLA TERRA, UNIVERSITÀ DEGLI STUDI DI MILANO, VIA BOTTICELLI 23, 20133, MILANO, ITALY

[2]ETH ZENTRUM, 8092, ZÜRICH, SWITZERLAND

[3]DEPARTMENT OF EARTH AND PLANETARY SCIENCES, AMERICAN MUSEUM OF NATURAL HISTORY, NEW YORK, NY 10024, USA

RECEIVED DECEMBER 10, 1999; REVISED TYPESCRIPT ACCEPTED JUNE 26, 2000

The phlogopite peridotite unit of the Finero Complex is a restitic harzburgite that records two metasomatic events. The first event is related to the intrusion of basaltic magma, which reacted with the pyroxene of the host harzburgite to produce chromitite pods with dunite haloes. It also produced secondary clinopyroxene and amphibole in the harzburgite and enriched harzburgite in Na and the light rare earth elements. The second metasomatic event is related to the later intrusion of clinopyroxenitic dykes. During this event, water-rich vapour penetrated the harzburgite along fractures and reacted with it to form phlogopite, thus enriching the rock in K. Chromitites host zircons that yield an age for the first metasomatic event of 207·9 + 1·7/−1·3 Ma, during which time extensional tectonics prevailed in the Southern Alps.

KEY WORDS: *metasomatism; chromitite; zircon; geochronology; Finero*

INTRODUCTION

The phlogopite peridotite of the Finero Complex hosts chromitite–dunite bodies that, although small, are the largest in the Alps. The chromite is magnesian and locally contains inclusions of Fe–Ni–Cu sulphide and platinum group element minerals (Ferrario & Garuti, 1990). Chromitite forms well-defined bodies with modal chromite concentrations as high as 75%. The occurrences were described by Roggiani (1948), Friedenreich (1956), Forbes *et al.* (1978) and Saager *et al.* (1982).

The petrology of the Finero Complex is poorly understood. One reason is that the phlogopite peridotite, which makes up the core of the complex, exhibits anomalous petrographic and geochemical characteristics indicative of metasomatism and of a multistage evolution (Coltorti & Siena, 1984; Cumming *et al.*, 1987;Voshage *et al.*, 1987; Hartmann & Wedepohl, 1993; Lu *et al.*, 1997*a*, 1997*b*). One aim of this study is to unravel the sequence of events that affected the phlogopite peridotite. The relationship between the mineralization and metasomatism was investigated by combining detailed petrographic observations with whole-rock data and electron and ion probe data on the compositions of individual phases. The discovery of accessory zircons within chromitite also allowed us to date the formation of the

*Corresponding author. Telephone: +39-02-23698342. Fax: +39-02-70638681. E-mail: giovanni.grieco@unimi.it

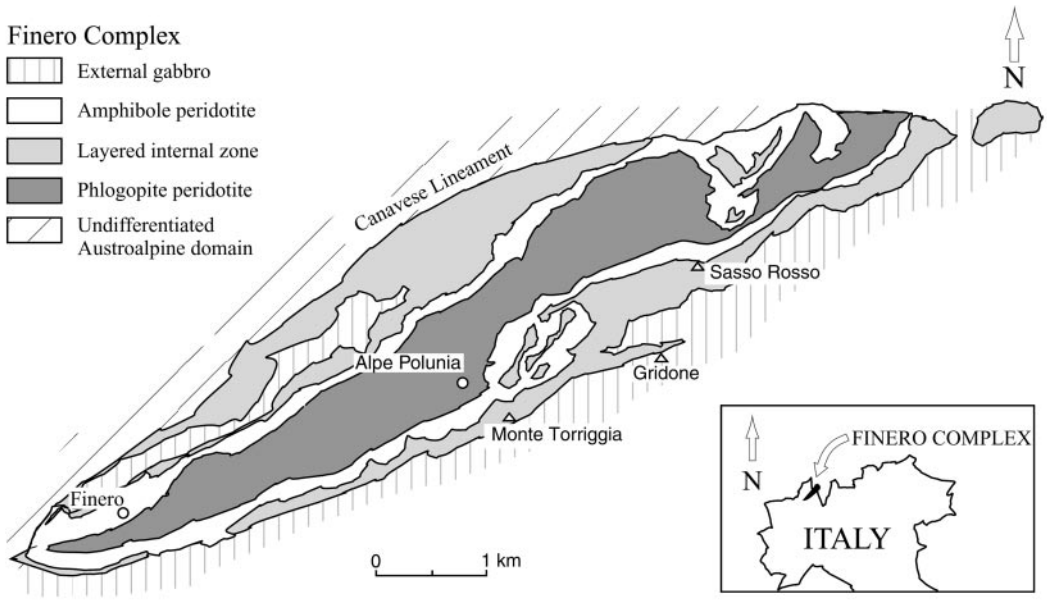

Fig. 1. Geological sketch map of the Finero Complex, Ivrea–Verbano Zone, northwestern Italy and southern Switzerland. Location of M. Torriggia is 46°08′48″N, 8°34′41″E.

chromitite and related metasomatic events and place them within the tectonic evolution of the southern Alps.

GEOLOGICAL AND PETROLOGICAL BACKGROUND

The Finero mafic–ultramafic complex crops out as a concentrically zoned elliptic body covering an area of about 12 km × 2·5 km in the northern section of the Ivrea–Verbano Zone (northwestern Italy). It occurs within high-grade metasediments (kinzigites, stronalites) and metavolcanic rocks and consists, from the core outward, of an amphibole- and phlogopite-bearing peridotite known as the phlogopite peridotite unit, a layered internal zone of ultramafic and mafic rocks, an amphibole peridotite and an external gabbro (Fig. 1).

The phlogopite peridotite unit, whose thickness is unknown, forms an elongated body (10 km × 1 km) at the core of the Finero Complex, whose tectonic setting is broadly an antiform with a SSW–NNE axis. Its main distinct lithology is amphibole- and phlogopite-bearing harzburgite. Patches of dunite are common and often form irregularly shaped bodies that are associated with chromitites. Clinopyroxenite dykes and rare alkali pegmatites crosscut the harzburgite. The original relationships are partially obscured by later Alpidic deformation. The layered internal zone is 50–130 m thick and consists of cyclic units of amphibole websterite, amphibole peridotite, garnet–amphibole gabbro and anorthosite in layers of centimetre to decimetre thickness. The rarely visible contacts to the phlogopite peridotite are usually affected by later tectonic events. The increasing content of modal olivine marks the transition from the layered internal zone to the amphibole peridotite, which is 200–300 m thick. This unit consists of dunite, wehrlite and lherzolite enriched in pargasitic amphibole. Thin layers of chromian spinel and patches of coarse-grained pargasite are locally found in this unit (Forbes *et al.*, 1978). The external gabbro is 100–150 m thick and consists of garnet–amphibole gabbro containing rare pyroxenitic and anorthositic layers. The boundary of the amphibole peridotite is marked by a gradual increase of plagioclase in the ultramafic rocks. The transition to the metasedimentary Kinzigitic Series is not clear because of the complex structural relationships that exist between the various lithologies of the Kinzigitic Series and the external gabbro.

The harzburgite of phlogopite peridotite comprises 60–90% olivine, 5–20% orthopyroxene, 0–5% clinopyroxene, 0–10% amphibole, 0–5% spinel and up to 15% phlogopite (Coltorti & Siena, 1984). It has been interpreted to represent a slice of mantle that was metasomatically enriched in incompatible elements and tectonically emplaced into the crust (Coltorti & Siena, 1984; Cumming *et al.*, 1987; Voshage *et al.*, 1987; Hartmann & Wedepohl, 1993; Lu *et al.*, 1997*a*, 1997*b*; Zanetti *et al.*, 1999). Cumming *et al.* (1987) concluded on the basis of Pb-isotope data that the ultramafic and gabbroic rocks of the Finero Complex originated from a mantle that was contaminated by dehydration reactions in a downgoing oceanic slab. On the basis of a much broader set of data,

Hartmann & Wedepohl (1993) concluded that the Finero peridotite was depleted in incompatible elements by the extraction of a basaltic melt. It was then heterogeneously enriched in incompatible elements by one, or possibly two, fluid pulses that derived from a subducted crustal slab. Zanetti *et al.* (1999) proposed that the metasomatic agent was a melt derived from an eclogite-facies slab; this melt infiltrated the overhanging harzburgitic mantle wedge and formed clinopyroxenite dykes.

ANALYTICAL METHODS

Chemical analyses of minerals were carried out using the ARL-SEMQ microprobe at the University of Milan. Operating conditions were 15 kV acceleration voltage, beam current of 20 nA for all elements and 3 μm spot size.

Rare earth element (REE) analyses of amphiboles and clinopyroxenes were carried out with the CAMECA IMS-3f ion probe at Woods Hole Oceanographic Institution. The primary beam was operated at a current of ~20 nA and focused to a spot of ~20 μm in diameter. An energy offset of the secondary ion beam of −60 V was employed. Accuracy was monitored by periodic analysis of Kilbourne Hole augite KH-1, the composition of which is known (Irving & Frey, 1984). The relative 2σ error based on several tens of analyses of KH-1 is ~15% for each REE. The data are presented normalized to the CI chondrite composition of Anders & Grevesse (1989).

Isotope analyses of zircons were carried out at ETH Zentrum, Zürich. Rock samples were crushed by hand and the zircon fragments handpicked under a binocular microscope. Some samples were air-abraded to eliminate marginal zones where Pb had been lost. Total Pb blanks for multigrain analyses ranged from 20 to 10 pg. The analytical procedures have been reported by von Quadt (1997).

RESULTS

Texture and petrography

The phlogopite peridotite is a composite unit made up of harzburgite, clinopyroxenite, dunite and chromitite. The high MgO values of harzburgitic bulk-rock samples coupled with relatively low concentrations of Al_2O_3, CaO and TiO_2 indicate its strongly restitic character (Grieco, 1998*a*). Compared with the two other main peridotitic bodies of the Ivrea–Verbano Zone, namely Balmuccia and Baldissero peridotites, Finero harzburgite is more depleted (Hartmann & Wedepohl, 1993; Zanetti *et al.*, 1999). The *mg*-number of olivine varies from 0·90 to 0·92, the *mg*-number of orthopyroxene from 0·91 to 0·92 and the *cr*-number of spinel from 0·48 to 0·60. The metasomatic processes that affected the phlogopite peridotite led to extreme modification of this original lithology by enrichment in incompatible elements and growth of new phases such as clinopyroxene, amphibole and phlogopite.

Clinopyroxenites form dykes of centimetre to decimetre thickness that are concordant with or slightly discordant to the main harzburgite foliation. Their contact with harzburgite is always sharp and marked by a strong colour contrast, so that they are a very distinctive feature in the field, even where rocks are altered. At the contact, reaction products between the clinopyroxenite and the host harzburgite and transitional changes in modal composition are not observed. Only in one outcrop at Alpe Polunia can a clinopyroxenite dyke be observed to transect a dunite body. The dykes contain clinopyroxene as the main constituent and minor but variable amounts of orthopyroxene, amphibole, phlogopite and rare olivine. All phases that are present both in the host harzburgite and in the clinopyroxenite dykes, except phlogopite, show more evolved compositions in the latter, indicating that the two rocks did not equilibrate with each other. Thus in the clinopyroxenite dykes *mg*-numbers are 0·87–0·88 for olivine, 0·89–0·90 for orthopyroxene, 0·92–0·94 for clinopyroxene and 0·87–0·89 for amphibole, whereas in harzburgite at the dyke contact *mg*-numbers are 0·91–0·93 for olivine, 0·91–0·92 for orthopyroxene, 0·95–0·96 for clinopyroxene and 0·89–0·91 for amphibole.

Dunite bodies are common and scattered throughout the phlogopite peridotite but they are much less evident in the field and virtually undistinguishable from harzburgite when altered. The dunites are composed of 90–95% modal olivine, the other minerals being spinel and orthopyroxene. Clinopyroxene and amphibole are locally present. The contact between the dunite and surrounding harzburgite is gradational and expressed in the changing modes of olivine and orthopyroxene. In the dunite olivine has *mg*-numbers of 0·93–0·96 and orthopyroxene has *mg*-numbers of 0·93–0·94 and TiO_2 contents of 0·07–0·10%; in the harzburgite the olivine *mg*-numbers are 0·89–0·92 and orthopyroxene has *mg*-numbers of 0·91–0·92 and TiO_2 contents of 0·01–0·04%.

The main occurrences of chromitite-bearing dunites are located in the marginal zones of phlogopite peridotite. The largest and best exposed outcrops occur in the southern part of the structure, at Alpe Polunia. The chromitite bodies form irregular pods, schlieren, elongated lenses and discontinuous layers up to 100 m long and 0·5 m thick. They were folded, boudinaged and locally affected by younger faulting. As noted above, the chromitites are surrounded by dunite. The contact between dunite and chromitite is always sharp.

Clinopyroxene and amphibole are inhomogeneously distributed in chromitites. Most chromitites contain both

phases, with modal concentrations up to 7 and 18%, respectively. Clinopyroxene and type I amphibole (see below) show primary magmatic relationships with olivine and chromite. The minor phases include olivine and orthopyroxene. The accessory phases include base metal sulphides, base metal alloys, platinum group element minerals, Ti oxides and zircons. Phlogopite is very rare in chromitites and crosscuts all the other phases. Type I amphibole is often observed to be corroded and replaced by a symplectitic assemblage of Cr-spinel (type III chromite) and phlogopite, possibly as a result of reaction of the original assemblage with metasomatizing fluid.

Mineral chemistry

Three textural types of chromite may be distinguished (Table 1, Fig. 2). Type I chromite consists of small, individual rounded grains scattered throughout harzburgite; type II chromite makes up the massive chromitites, is coarse grained and chemically zoned and has greater *cr*-number, *mg*-number and TiO_2 contents (>0·25%) than other chromite types; type III chromite is composed of small, irregular-shaped Cr-spinel grains in symplectites around type I amphibole grains. Type II chromite grains commonly exhibit peculiar zoning patterns. Where they are in contact with olivine (Fig. 3a), the grain rims are depleted in Cr_2O_3 by up to 7% compared with their cores. In grains in contact with orthopyroxene (Fig. 3b) and type I amphibole the zoning is reversed, with the chromite rims containing as much as 63% Cr_2O_3 and enriched in Cr_2O_3 by up to 10% relative to the cores. A single chromite grain can thus show different core–rim zonings depending on the contacting silicate minerals. An enrichment in Cr_2O_3, usually accompanied by depletion in MgO, is also present around micro-fractures within chromite grains in chromitite samples containing abundant clinopyroxene and amphibole. This shows that the enrichment in Cr_2O_3 followed the growth and fracturing of chromite grains and was superimposed on a previous zoning pattern characterized by depletion of Cr_2O_3 from core to the rim. Finally, where they are in contact with clinopyroxene (Fig. 3c), chromite grains are enriched in Cr_2O_3 and isolated from pyroxene by amphibole II. Platinum group mineral inclusions within chromite grains are abundant and platinum group element concentrations of chromitite are high in clinopyroxene and amphibole-free chromitite, whereas in clinopyroxene and amphibole-rich chromitite, where Cr_2O_3 depletion from core to rim is the most common zoning of chromite, platinum group mineral inclusions within chromite grains are absent or very rare and platinum group element concentrations of chromitite are low (Grieco, 1998*b*). This suggests that the metasomatic agent, which reversed the zoning of chromite grains, was able to dissolve already formed platinum group mineral grains.

Distinction of three different types of amphiboles is based on textural relationships and composition. Type I refers to equant crystals in chromitite, dunite and harzburgite but not in clinopyroxenite. Type II amphibole is present only in chromitite as a thin film between chromite and clinopyroxene grains and as replacing phase along the structural planes of clinopyroxene; only rarely, in the most strongly metasomatized zones, does amphibole II occur as equant grains. Type III amphibole is found in clinopyroxenite and in harzburgite at the contact with clinopyroxenite dykes. All three amphibole types can be classified as pargasitic to edenitic hornblende (Table 2, Fig. 4), although they differ in minor elements and *mg*-number (Fig. 5). Type I is low in TiO_2 (<0·70%) and relatively high in K_2O (0·35–1·10%) contents; type II contains more TiO_2 (1·60–1·80%) and less K_2O (<0·20%); and type III is more evolved than both type I and II, with lower *mg*-number (<0·895 vs 0·903–0·920 for type I and 0·915–0·933 for type II amphibole).

Rare earth element geochemistry

At Finero the least metasomatized harzburgite samples show the most depleted whole-rock REE patterns. These rocks have lower normalized light rare earth element [$(LREE)_N$] values (0·07–0·7) (Fig. 6) than peridotites of Balmuccia and Baldissero. On the other hand, $(LREE)_N$ values (0·8–20) of the most metasomatized harzburgite samples are higher than those of the Balmuccia and Baldissero peridotites (0·2–1) (Hartmann & Wedepohl, 1993). Chromitite is systematically enriched in LREE relative to all harzburgite samples (Table 3, Fig. 6). Thus, in the former La ranges from 0·86 to 3·26 ppm and $(La/Yb)_N$ from 29·8 to 112·8, whereas in harzburgite the respective ranges are 0·07–0·67 ppm and 4·4–16·6.

All three types of amphiboles show strong LREE enrichment (Table 4, Fig. 7), with $(La/Yb)_N$ ranging between 6·39 and 25·62, but differ in total REE contents. Type I amphiboles are lower and more variable in LREE contents and exhibit slightly higher Eu anomalies compared with type II and III amphiboles. The main distinction, however, concerns the Nd value, defined as $Nd^* = Nd_N/SQRT(Ce_N \times Sm_N)$. Type I and II amphiboles have Nd* <1 whereas type III amphiboles have Nd* >1, resulting in a concave-upward LREE pattern for types I and II and a concave-downward pattern for type III amphibole.

Although the major element compositions of clinopyroxene in chromitite and harzburgite are similar, their REE patterns strongly differ (Table 4, Fig. 8). Relict clinopyroxene grains in restitic harzburgite show the lowest LREE contents and the lowest $(La/Yb)_N$ values (2·7

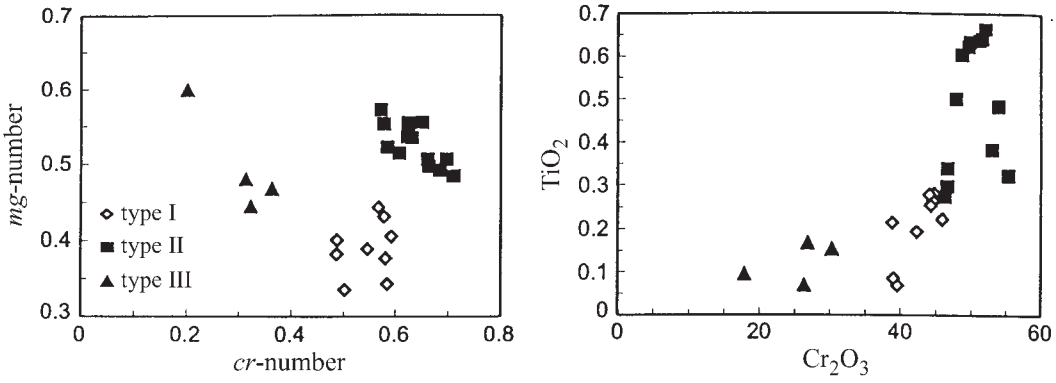

Fig. 2. *cr*-number vs *mg*-number and Cr_2O_3 vs TiO_2 diagrams of Finero chromites. (See text for descriptions of types I, II and III.)

and 3·1). Later-formed subhedral clinopyroxene grains in both harzburgite or chromitite show higher LREE contents and $(La/Yb)_N$ values (8·1–16·0), with patterns similar to those of type I amphibole. Rare clinopyroxene grains, growing on and thus post-dating orthopyroxene within chromitites, show the highest LREE contents but $(La/Yb)_N$ values (8·6 and 12·5) comparable with early formed clinopyroxene. Finally, clinopyroxene grains of clinopyroxenite show patterns similar to those within chromitite but with lower $(La/Ce)_N$ values (0·99 vs 1·14–1·44).

Zircon U–Pb data

Zircons are irregularly distributed within the chromitites. In polished sections, 10–25 grains, with dimensions of up to 600 μm across, were observed in areas of <50 mm^2. Zircon grains also occur aligned parallel to chromite bands. Most grains are subhedral to anhedral and often observed to form aggregates of up to four crystals between olivine and chromite. No zoning is visible, and the zircons are virtually free of inclusions. The petrographic relations suggest that the zircons crystallized together with the main constituents of the chromitite from a partial melt. Cathodoluminescence revealed curved, mostly diffuse zoning patterns that do not reflect the crystal outlines (Fig. 9). No relics of oscillatory zoning were observed. The relatively high and heterogeneous trace element distribution and the absence of relics of oscillatory zoning support zircon crystallization from a volatile-rich magma.

Four grain-size fractions, which also included fragments of originally larger crystals, were analysed. The U concentrations vary between 1120 and 1240 ppm (Table 5).

The regression line (Fig. 10) yields an upper intercept age of 207·9 + 1·7/−1·3 Ma and a lower intercept at −7 ± 71 Ma. The slightly discordant ages of the largest and smallest size fractions indicate a mild disturbance of their U–Pb systems, which, according to the lower intercept age, occurred recently, possibly in the laboratory. There is no evidence of an inherited age, and thus the upper intercept age is taken as the age of zircon crystallization.

The age of 207·9 + 1·7/−1·3 Ma is significantly higher than the age of 195 ± 4 Ma that we obtained on zircons from an alkali pegmatite intruding phlogopite peridotite at Rio Creves, in the northern portion of the Finero Complex. From the pegmatite Stähle *et al.* (1990) reported a zircon evaporation age of 225 ± 13 Ma. Zircons from a pegmatitic plagioclase vein at the contact between the hornblende peridotite and the external gabbro in Val Boschetto (northeastern portion of the complex) did not yield a dataset that defines a precise age. However, from one fraction we obtained within the error limits a concordant age of 202 ± 1 Ma, which contrasts with the concordant age of 212·5 ± 0·5 Ma obtained by Oppizzi & Schaltegger (1999) in zircon fragments from a similar vein in the neighbouring Val di Capolo. These data will be discussed elsewhere.

DISCUSSION

Petrogenesis

Dunite has been frequently observed to envelop chromitite bodies in tectonized peridotites (Augè, 1987; Leblanc & Ceuleneer, 1992; Leblanc & Nicolas, 1992; Melcher *et al.*, 1997). The presence of restitic dunites containing Cr-spinel may result from partial melting of spinel peridotite, followed by melt extraction (Jaques & Green, 1980). This mechanism does not explain the field relations at Finero, however. Another possibility relates the formation of dunites to the assimilation of pyroxene by an olivine-saturated melt intruded from greater depth (Kelemen, 1990*a*). The reaction is driven by the fact that melt, which would have been in equilibrium with peridotite at greater depth, is not in equilibrium with the lower-pressure and cooler peridotite. Upon intrusion, the melt thus reacts with both clinopyroxene and

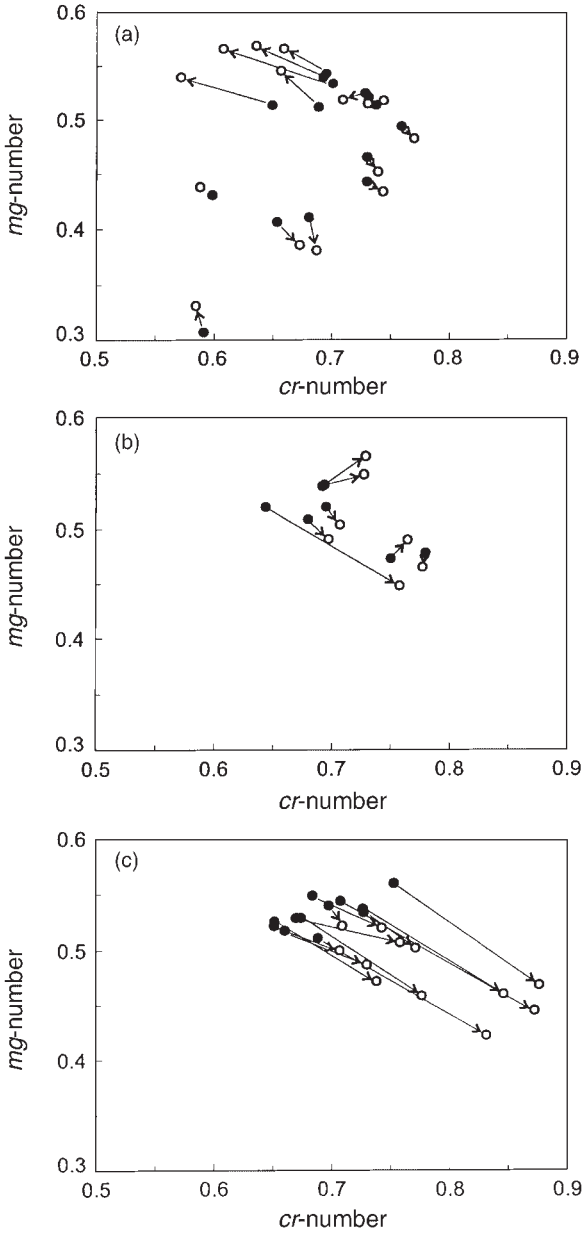

Fig. 3. *cr*-number vs *mg*-number core–rim zoning of Finero chromitites as a function of the contact mineral: (a) olivine; (b) orthopyroxene; (c) clinopyroxene.

orthopyroxene of the host rock to produce olivine. (Kelemen, 1990*a*, 1990*b*; Kelemen *et al.*, 1992). The formation of dunite is also enhanced by the presence of water, which expands the field of olivine stability at the expense of that of pyroxene (Kushiro, 1969, 1972). Chromite may also crystallize during the process, simply because of the enrichment of the residual melt in SiO_2 as olivine crystallizes (Zhou *et al.*, 1994; Zhou & Robinson, 1997). This process may also be enhanced by the presence of water because water lowers the liquidus of silicate minerals much more than that of chromite and thus has the effect of expanding the stability field of chromite (Nicholson & Mathez, 1991).

Several observations argue for such an origin of the dunite–chromitite assemblage in the Finero phlogopite peridotite and relate to this process the widespread crystallization of clinopyroxene and amphibole. First, clinopyroxene and amphibole are virtually absent in dunites but abundant, albeit heterogeneously distributed, in the harzburgite and hence their crystallization cannot be related to a later event that affected both lithologies. In the harzburgite, REE patterns indicate that both primary and metasomatic clinopyroxene are present. Second, dunite and chromitite always occur together. Also, the REE contents and LREE/HREE (heavy REE) ratios of the chromitites are systematically higher than those of the harzburgite, suggesting that chromitite formation is related to the first metasomatic episode that affected the phlogopite peridotite. Therefore, the dunite must be related to this event also. Third, the high TiO_2 contents and correlated Mg and Cr contents of chromite in the chromitites are consistent with their crystallization from melt. In contrast, type I chromite in the harzburgite is interpreted as the original spinel that was enriched in Cr and depleted in Ti during melt extraction from harzburgite. That happened, of course, well before the rocks were metasomatized by mafic melt.

Clinopyroxene, amphibole and zircon crystallized from the residual melt, which may also have become vapour saturated at some point during the evolution, although there are no specific features of the rock to indicate whether or when this might have happened. In any case, the continued reaction of the last residual melt with the solid assemblage under conditions of low melt/rock ratio resulted in (1) the enrichment of chromite in Cr and Mg, and (2) the crystallization of films of type II amphibole at chromite–clinopyroxene boundaries. Orthopyroxene and clinopyroxene were consumed by this metasomatic reaction, as proposed by Neal (1988) for New Caledonia peridotites. A reaction for Mg end members can be written as

$$24MgAlCrO_4 + 16CaMgSi_2O_6 + 14Mg_2Si_2O_6 + 8H_2O + 4Na_2O \rightarrow 8NaCa_2Mg_4Al_3Si_6O_{12}(OH)_2 + 12MgCr_2O_4 + 12Mg_2SiO_4.$$

This accounts for the peculiar zoning of the Finero chromitites as a function of the silicate assemblage around them. Cr_2O_3 depletion in chromite from core to the rim is a common feature of chromite crystallized from melt (Leblanc & Ceuleneer, 1992), and is related to an early stage of crystallization, with contemporaneous formation of olivine. During a later stage of crystallization, after the growth of pyroxenes and type I amphibole, intergranular films of melt were able to change the rim composition

Table 1: Representative analyses of chromite (wt %) from Finero phlogopite peridotite

	Type I chromite						Type II chromite										Type III chromite			
	cv3a-c	cv3a-r	pr1a-c	pr1a-r	cvr1-c	cvr1-r	cv8a-c	cv8a-r	b1c-c	b1c-r	cv8c-c	cv8c-r	b1d-c	b1d-r	b1e-c	b1e-r	cv3b	cv3c	pr1c	b1b
Contact mineral:		olv		olv		opx		olv		olv		opx		cpx		cpx				
Constituent	core	rim	core	rim	core	rim	core	rim	core	rim	core	rim	core	rim	core	rim				
SiO_2	0·03	0·01	0·66	0·16	0·17	0·19	0·01	0·00	0·06	0·06	0·01	0·02	0·06	0·08	0·03	0·05	0·04	0·05	0·33	0·14
TiO_2	0·20	0·23	0·09	0·07	0·25	0·23	0·49	0·47	0·34	0·44	0·49	0·24	0·34	0·28	0·28	0·21	0·09	0·12	0·07	0·06
Al_2O_3	21·54	22·79	23·04	23·22	17·93	18·95	15·88	18·43	18·97	23·42	15·88	8·52	18·70	14·49	18·57	14·27	41·73	33·41	34·15	54·74
Cr_2O_3	41·49	40·72	39·09	39·57	44·01	42·78	48·11	46·11	46·06	40·33	48·11	58·00	46·00	50·05	46·74	51·23	20·74	27·40	26·32	11·76
Fe_2O_3	6·32	5·74	4·00	4·89	6·36	5·90	5·93	5·75	5·93	6·83	5·93	3·26	5·96	6·26	5·51	4·72	5·42	7·18	6·83	0·91
FeO	21·19	20·92	25·82	24·77	21·09	23·29	17·81	16·82	18·15	17·65	17·81	20·00	17·74	17·92	17·92	18·25	19·30	21·50	20·65	14·26
MnO	0·30	0·35	0·44	0·37	0·34	0·44	0·27	0·27	0·27	0·26	0·27	0·30	0·27	0·36	0·27	0·26	0·17	0·30	0·28	0·12
NiO	0·04	0·20	0·11	0·09	0·16	0·13	0·00	0·00	0·19	0·08	0·00	0·00	0·16	0·07	0·09	0·09	0·00	0·00	0·14	0·29
MgO	9·23	9·46	6·59	7·02	8·68	7·31	10·87	11·80	11·19	12·11	10·87	8·45	11·32	10·55	11·19	10·14	12·32	10·01	10·74	17·00
CaO	0·02	0·00	0·02	0·03	0·03	0·03	0·01	0·00	0·01	0·00	0·01	0·00	0·01	0·18	0·01	0·17	0·01	0·01	0·13	0·02
Na_2O	0·01	0·00	0·02	0·00	0·01	0·03	0·00	0·01	0·00	0·00	0·00	0·00	0·00	0·00	0·00	0·00	0·08	0·07	0·02	0·00
K_2O	0·00	0·00	0·00	0·00	0·00	0·00	0·01	0·01	0·00	0·00	0·01	0·00	0·00	0·00	0·00	0·00	0·00	0·00	0·00	0·00
Total	100·37	100·41	99·88	100·19	99·03	99·28	99·38	99·67	101·17	101·18	99·38	98·80	100·56	100·24	100·60	99·39	99·90	100·05	99·65	99·30

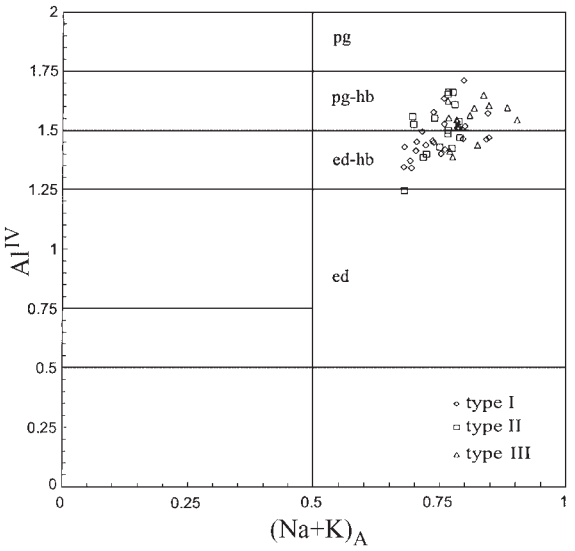

Fig. 4. Analyses of amphiboles in an Al^{IV} vs $(Na + K)_A$ diagram.

of chromite, enriching it in Cr_2O_3, according to the above reaction. The result is a mosaic-like zoning where a single grain of chromite can show both depletion and enrichment of Cr_2O_3 from core to the rim, depending on the phase in contact with any portion of the rim.

There is no evidence to relate the formation of phlogopite to the processes that gave rise to the formation of the dunite–chromitite bodies. Phlogopite is very rare in

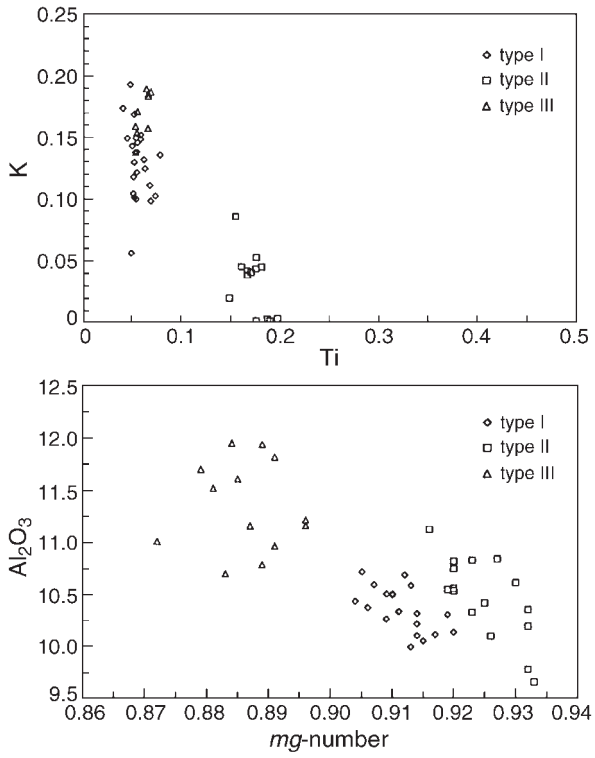

Fig. 5. Amphibole compositions in a Ti vs K diagram and in an *mg*-number vs Al_2O_3 diagram.

Table 2: Representative analyses of amphiboles (wt %) from Finero phlogopite peridotite

	Type I					Type II					Type III				
Component:	b1a	cv3a	cv3b	pr1a	cv6a	c2a	c1a	c1b	c3a	c3b	cv2a	cv2b	cv2c	f1a	f1b
SiO_2	45·40	45·22	44·63	44·80	45·72	45·83	44·63	44·52	45·61	44·83	44·38	45·19	44·40	46·00	46·09
TiO_2	0·49	0·50	0·51	0·45	0·49	1·76	1·70	1·64	1·59	1·83	0·61	0·64	0·61	0·64	0·72
Al_2O_3	10·27	11·17	11·82	11·92	10·59	10·35	10·83	10·82	10·19	10·61	11·61	11·52	10·97	11·01	11·16
Cr_2O_3	1·97	1·84	1·70	2·05	2·07	2·00	1·94	1·95	1·76	2·48	2·03	1·88	2·32	1·73	2·04
FeO*	3·65	3·98	4·23	3·33	3·55	2·51	3·08	3·16	2·78	2·76	4·13	4·34	4·14	4·67	4·01
MnO	0·05	0·06	0·05	0·03	0·02	0·00	0·02	0·05	0·06	0·02	0·08	0·05	0·05	0·06	0·03
MgO	19·56	18·49	18·63	18·92	19·80	19·28	19·74	19·68	20·10	19·68	17·81	18·07	18·58	17·81	17·73
CaO	12·47	13·18	12·56	12·92	12·47	13·04	12·54	12·31	12·88	12·87	12·81	12·73	12·29	12·47	12·41
Na_2O	2·36	2·20	2·21	2·05	2·15	2·77	2·65	2·61	1·99	2·18	2·50	2·59	2·27	2·32	2·21
K_2O	0·71	0·87	0·84	1·06	0·93	0·02	0·25	0·24	0·83	0·93	1·00	1·02	0·99	0·68	0·87
H_2O	2·10	2·10	2·10	2·11	2·12	2·11	2·11	2·10	2·12	2·12	2·08	2·10	2·08	2·09	2·09
Total	99·03	99·60	99·28	99·64	99·91	99·67	99·48	99·08	99·91	100·31	99·04	100·13	98·70	99·48	99·36

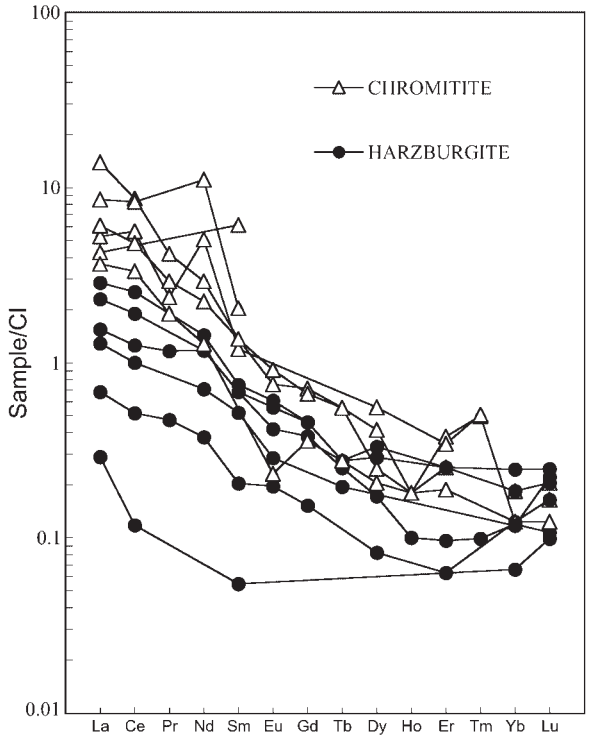

Fig. 6. Whole-rock chondrite-normalized REE patterns of chromitite and harzburgite.

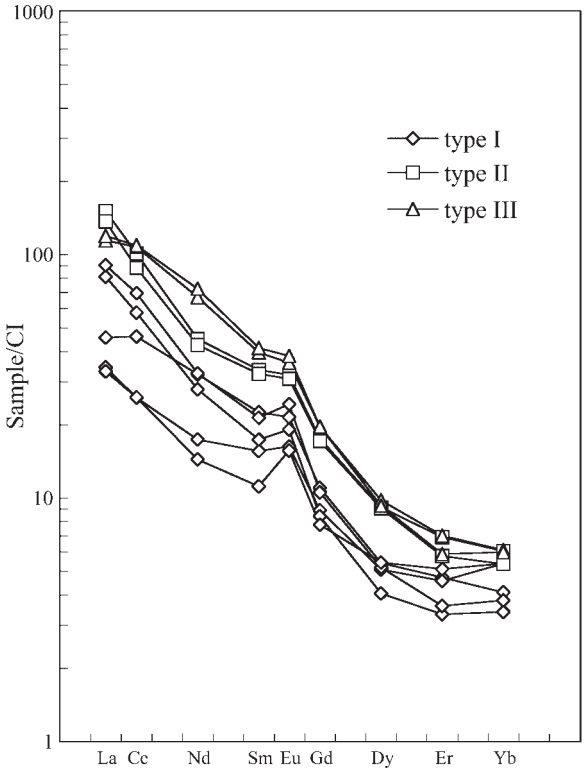

Fig. 7. Chondrite-normalized REE patterns of amphibole.

these lithologies. Textural evidence points to a later crystallization of phlogopite under different conditions. The phlogopite and Cr-spinel symplectites associated with type I amphibole show that phlogopite formed under disequilibrium conditions after the crystallization of type I amphibole. This suggests a later, perhaps independent metasomatic event.

Phlogopite is a common mineral in the clinopyroxenitic

Table 3: REE and trace elements (ppm) of Finero phlogopite peridotite

Lithology:	harz. PO2AB	harz. CV3	chrom. PO2C	chrom. C2	chrom. C2a	chrom. B1a	chrom. B1b	chrom. B2
La	0·16	0·364	0·86	1	1·229	1·42	2	3·26
Ce	0·31	0·759	2·01	n.d.	3·39	2·89	5	5·22
Pr	0·042	0·104	0·17	n.a.	0·2101	0·259	n.a.	0·373
Nd	0·17	0·534	0·58	n.d.	2·289	1·01	5	1·32
Sm	0·03	0·1	0·01	0·9	0·1759	0·2	0·3	0·2
Eu	0·011	0·0234	0·013	n.d.	n.a.	0·051	n.d.	0·042
Gd	0·03	0·0748	0·07	n.a.	0·902	0·13	n.a.	0·14
Tb	0	0·00909	0·01	n.d.	n.a.	0·02	n.d.	0·02
Dy	0·02	0·0417	0·05	n.a.	0·1348	0·1	n.a.	0·06
Ho	0	0·00557	0·01	n.a.	0·17	0·01	n.a.	0·01
Er	0·01	0·0153	0·03	n.a.	0·0545	0·04	n.a.	0·06
Tm	0	0·00239	0	n.a.	0·0363	<0·005	n.a.	0·012
Yb	0·02	0·0194	0·02	n.d.	n.a.	0·03	n.d.	0·02
Lu	0·004	0·0026	0·003	n.d.	0·0226	0·005	n.d.	0·004
Ba	0·9	32	2·9	n.d.	21	6·3	n.d.	1·6
Co	128	108	106	190	178	112	97	139
Cr	4929	2965	3748	21000	156000	1945	2900	72480
Ni	3577	2383	2152	910	1040	1637	1800	1266
Rb	0·3	6·17	0·7	n.d.	n.d.	0·6	n.d.	0·5
Sb	0·12	0·04	0·13	n.d.	1·1	0·13	n.d.	0·19
Sc	1	n.d.	1	7·4	n.d.	6	8·8	n.d.
Sr	0·91	8·31	6·24	n.d.	9·09	21·8	n.d.	6·01
V	11	25·3	13	n.a.	677	20	n.a.	215
Y	0·1	0·17	0·3	n.a.	0·28	0·4	n.a.	0·2
Zn	43	47·9	47	752	573	62	66	252
Zr	19	2·3	1·5	n.d.	6·33	50	n.d.	57

dykes that, at least in one case, were observed to crosscut dunite. Phlogopite crystallization in the harzburgite is attributed to the percolation of a later, water-rich melt from which clinopyroxenite dykes crystallized. The melt penetrated the host rock along structural planes, accounting for the much more heterogeneous and structurally controlled distribution of phlogopite than of clinopyroxene and amphibole. This argues also for a lower temperature for this second metasomatic event.

The very high REE and LREE/HREE ratio of clinopyroxenite is due to their high clinopyroxene content. The final, water-rich melt, which metasomatized the harzburgite, although rich in incompatible elements such as K, was not strongly enriched in LREE. This is because the $D^{cpx/melt}$ of LREE is much higher than $D^{olv/melt}$ or $D^{chr/melt}$, so, although crystallization of chromite and olivine in the dunite–chromitite assemblage can account for an early increase of LREE content of melt, crystallization of large amounts of clinopyroxene in the clinopyroxenite dykes would not have resulted in such an increased content of LREE in the residual melt. Thus, the metasomatizing melt did not greatly modify the original absolute or relative REE contents of the peridotites, and it resulted in phlogopite that is not particularly enriched in REE.

The Sr and Nd isotope data reported by Voshage *et al.* (1987), Hartmann & Wedepohl (1993) and Lu *et al.* (1997) show mantle signatures for the external gabbro (except a few outliers), the amphibole peridotite, the layered internal zone, the phlogopite-free harzburgite and the alkali pegmatite (Stähle *et al.*, 1990) ($^{87}Sr/^{86}Sr$ = 0·7026–0·7047, $^{143}Nd/^{144}Nd$ = 0·5125–0·5133), although a small crustal contribution (<10%) cannot be ruled out. By contrast, the phlogopite-bearing harzburgite shows a clear crustal imprint ($^{87}Sr/^{86}Sr$ = 0·70625–0·70832, $^{143}Nd/^{144}Nd$ = 0·5122–0·5123). Pb isotope ratios are sensitive to crustal contamination and the Pb isotopic compositions of all lithologies of the Finero

Table 4: Major elements and REE of amphiboles and clinopyroxenes of Finero phlogopite peridotite

Lithology:	Peridotite Type I					Chromitite Type II		Clinopyroxenite Type III	
	b1a1	cv3b5	cv1a	pr1b1	b1b13	c2a22	c2a25	cv2b3	cv2b2
Amphiboles									
SiO_2	45·37	44·63	45·2	44·01	45·97	45·68	45·83	44·46	44·4
TiO_2	0·48	0·51	0·73	0·38	0·55	1·5	1·76	0·59	0·61
Al_2O_3	10·51	11·82	10·69	12	10·22	10·55	10·35	10·79	10·97
Cr_2O_3	1·9	1·7	1·76	2·06	1·89	1·37	2	2·23	2·32
FeO*	3·41	4·23	3·44	3·8	3·26	3·02	2·51	4·18	4·14
MnO	0·05	0·05	0·02	0·04	0	0·03	0	0·07	0·05
MgO	19	18·63	19·32	19·18	19·27	19·25	19·28	18·51	18·58
CaO	12·43	12·56	12·64	12·39	12·48	12·65	13·04	12·22	12·29
Na_2O	2·61	2·21	2·34	2·25	2·2	2·6	2·77	2·21	2·27
K_2O	0·64	0·84	0·74	0·95	0·81	0·25	0·02	1·02	0·99
H_2O	2·08	2·1	2·1	2·1	2·09	2·1	2·11	2·07	2·08
Total	98·48	99·28	98·98	99·16	98·74	99·00	99·67	98·35	98·70
La	19·0194	7·7622	10·6964	8·0580	23·2206	38·9249	35·2523	26·7527	27·9549
Ce	34·7986	15·5942	27·7248	15·5600	45·9242	66·8892	58·3036	64·6075	65·7288
Nd	12·6495	6·4898	14·5269	7·8626	16·1343	22·3378	21·1041	30·1979	32·6644
Sm	2·5579	1·6424	3·3027	2·2857	3·4551	5·4096	5·2311	5·8131	6·0714
Eu	1·0667	0·8743	1·2035	0·9079	1·494	1·9653	1·8963	2·0067	2·1437
Dy	0·9850	1·3131	1·3100	1·2328	1·3784	2·4434	2·4188	2·3695	2·2505
Er	0·5270	0·8090	0·7473	0·7250	0·6291	1·204	1·0047	1·1127	0·9341
Yb	0·5524	0·8712	0·6637	0·8736	0·6775	1·0766	0·9527	0·9900	0·9729

Lithology:	Peridotite				Chromitite				Clinopyroxenite
	cv3b4	cv3b3	cv1b	b1a6	c2a	b2b3	b2b2	c3b1	cv2b1
Clinopyroxenes									
SiO_2	53·87	54·17	53·04	54·08	53·08	54·05	54·51	53·9	53·22
TiO_2	0·05	0·04	0·12	0·1	0·17	0·12	0·1	0·17	0·11
Al_2O_3	1·16	0·64	1·39	0·93	0·95	0·72	0·58	0·96	1·28
Cr_2O_3	0·47	0·39	0·82	0·51	0·59	0·59	0·58	0·65	0·69
FeO	1·95	1·78	2·46	1·98	1·86	1·61	1·51	1·78	2·48
MnO	0·04	0·02	0·08	0·09	0·01	0·07	0·03	0·4	0·08
MgO	17·39	17·53	17·39	17·96	17·63	18·2	18·19	18·21	17·28
CaO	25·08	25·27	24·22	24·59	24·1	24·01	23·99	24·27	23·83
Na_2O	0·21	0·11	0·35	0·21	0·27	0·37	0·29	0·27	0·28
K_2O	0	0	0	0·01	0	0·01	0	0	0
Total	100·22	99·95	99·87	100·45	98·66	99·75	99·78	100·61	99·24
La	1·2041	1·1413	3·5333	2·8090	10·6707	16·8273	24·6218	9·8722	8·6262
Ce	2·4948	2·4743	9·8541	6·3328	19·0440	58·1547	77·7806	16·3414	22·2429
Nd	1·4551	1·2399	5·5491	3·1716	8·4203	38·4605	45·0046	7·5167	11·5397
Sm	0·6281	0·4779	1·3428	0·6125	1·9641	8·5195	11·8080	2·4033	2·7820
Eu	0·1973	0·1374	0·3512	0·1916	0·6012	2·4058	2·9066	0·4296	0·6026
Dy	0·4227	0·3496	0·6593	0·3228	1·0288	3·5189	3·6905	0·8177	0·8770
Er	0·2562	0·4150	0·4149	0·2068	0·4199	1·4039	1·5325	0·6376	0·5820
Yb	0·3113	0·2512	0·3012	0·1684	0·4665	1·3482	1·3591	0·4255	0·4449

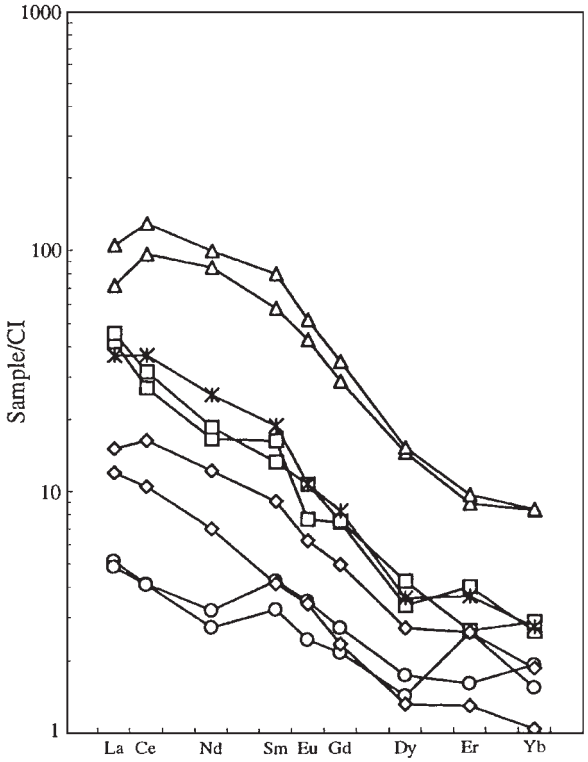

Fig. 8. Chondrite-normalized REE patterns of clinopyroxene: ○, small equant grains within harzburgite; ◇, larger subhedral grains within harzburgite; □, larger subhedral grains within chromitites; △, rare grains growing on orthopyroxene within chromitites; *, subhedral grains within clinopyroxenite.

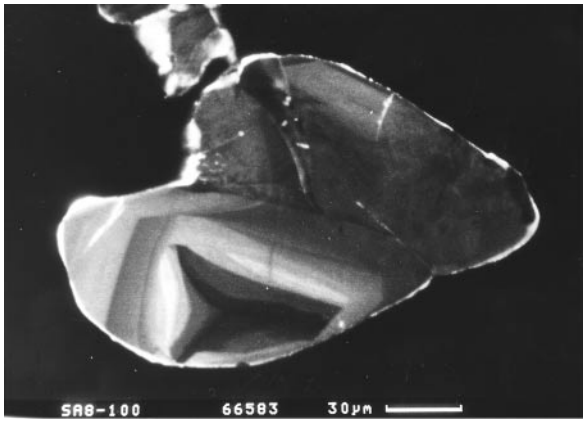

Fig. 9. Curved zoning of zircon, which does not follow the outlines of the crystal.

Complex [$^{206}Pb/^{204}Pb$ = 17·99–18·75, $^{207}Pb/^{204}Pb$ = 15·58–15·95; Cumming *et al.* (1987) and V. Koeppel, unpublished data, 1998] are intermediate between those of depleted mantle and the metasediments of the Ivrea Zone. The Pb of phlogopite from the phlogopite peridotite is, in accordance with Sr and Nd isotopic data, distinctly more crustal ($^{206}Pb/^{204}Pb$ = 18·58, $^{207}Pb/^{204}Pb$ = 15·625). The absence of Pb contamination in the rocks enveloping the Pb-contaminated phlogopite peridotite argues strongly against Pb transport by metamorphic fluids coming from the metasedimentary cover. Hence the source of metasomatic fluids that affected the phlogopite peridotite can be attributed to a contaminated mantle.

Age relations

The geochronology of the Finero Complex is poorly known. Voshage *et al.* (1987) reported a Rb–Sr whole-rock isochron from six phlogopite-bearing peridotites and one phlogopite pyroxenite that yielded an age of 293 ± 13 Ma and an initial $^{87}Sr/^{86}Sr$ of 0·7063 ± 0·0006. They interpreted this as the age of K metasomatism. From paired phlogopite–amphibole samples, Hartmann & Wedepohl (1993) obtained Rb–Sr ages ranging from 225 ± 5 to 163 ± 4 Ma and with $^{87}Sr/^{86}Sr_I$ of 0·7061–0·7082. However, amphiboles from phlogopite-free samples have $^{87}Sr/^{86}Sr$ ratios varying from 0·7031 to 0·7034.

Hunziker (1974) reported a K–Ar age defined by phlogopite and hornblende of 180 Ma, which is identical to the Rb–Sr phlogopite age. Individual K–Ar ages of amphibole as well as phlogopite appear to be biased by excess ^{40}Ar. They range from 206 to 220 Ma for phlogopite and exceed 1200 Ma for hornblende (Hunziker, 1974).

Lu *et al.* (1997) tentatively interpreted whole-rock Sm–Nd data from the amphibole peridotite as defining an isochron with an age of 533 ± 20 Ma, which is consistent with the Pb–Pb zircon evaporation age of 549 ± 12 Ma from the layered internal zone. Sm–Nd data of garnet, clinopyroxene, plagioclase and amphibole from the layered internal zone yielded internal isochrons indicating a concordant age of 215 ± 15 Ma, which was attributed to a reheating event in which temperatures exceeded 600°C.

As already mentioned, the textural evidence indicates that zircon grew late in the crystallization history of chromitite. The zircon age of 207·9 + 1·7/−1·3 Ma thus dates the crystallization of the chromitites and hence the first metasomatic episode. The formation of the alkali pegmatite at Rio Creves (195 ± 4 Ma) post-dates the age of the chromitite formation. The zircon ages of pegmatitic plagioclase veins in Val Boschetto and Val di Capolo indicate that their formation covered a considerable time span that overlaps the formation of the chromitites. Thus, magmatic activities covering a time span of ~20 my occurred in the Ivrea Zone during the Triassic period of rifting in the southern Alps. This event is also recorded elsewhere in the Ivrea Zone by zircon and monazite ages of 210–220 Ma (Vavra *et al.*, 1996).

Table 5: U and Pb concentrations and isotopic ratios for different zircon fractions

Sample	Fraction (μm)	Wt (mg)	U (ppm)	Pb_{rad} (ppm)	Pb_{com} (ppm)	$^{206}Pb/^{204}Pb$	$^{208}Pb/^{204}Pb$	$^{207}Pb/^{204}Pb$	$^{206}Pb/^{238}Pb$	$^{207}Pb/^{235}Pb$	$^{207}Pb/^{206}Pb$	$^{206}Pb/^{238}Pb$	$^{207}Pb/^{235}Pb$	$^{207}Pb/^{206}Pb$	ρ
RM 86															
1076	>100	3·25	1121	40·290	0·248	8288	1113·00	430·940	0·03551	0·24615	0·05027	224·9	223·4	207·5	0·95
1071	75–100	1·42	1186	36·510	0·611	3500	444·70	190·560	0·03230	0·22397	0·05030	204·9	205·2	208·8	0·98
1077	53–75	1·76	1193	39·480	0·561	4138	575·30	222·190	0·03258	0·22548	0·05020	206·6	206·5	204·1	0·97
1078	<53	1·79	1236	40·430	0·656	3642	528·70	197·700	0·03204	0·22218	0·05030	203·2	203·7	208·8	0·98

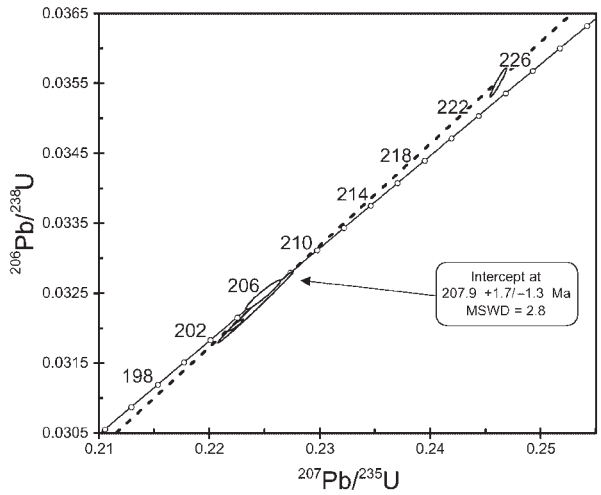

Fig. 10. $^{207}Pb/^{235}U$ vs $^{206}Pb/^{238}U$ regression line of Finero zircons.

The chromitite zircon age of 208 Ma is a maximum age for the clinopyroxenite dykes because at least one has been observed to be intrusive into a dunite.

CONCLUSIONS

Petrographic and chemical data on Finero phlogopite peridotite indicate two metasomatic events. One is related to the formation of dunite and chromitite bodies 208 ± 2 my ago and the other to the formation of clinopyroxenite dykes. These dunite–chromitite bodies formed by the reaction of mafic melt and the host peridotite. Clinopyroxene and amphibole crystallized from the residual melt, which also invaded the harzburgite to produce amphibole and enriched the rock in Na and incompatible elements (LREE). The evolving melt also affected the chromites by reversing their magmatic zoning.

The second event is the intrusion of the phlogopite-bearing clinopyroxenite dykes. The melt hardly interacted with the host rock and did not equilibrate with the host harzburgite. This behaviour may indicate that the process occurred at a relatively shallow crustal level and a low temperature. Interaction with the host rock was mainly restricted to K metasomatism of the peridotite, phlogopite being the result of metasomatic interaction. The growth of phlogopite is structurally controlled, and always related to the last ductile deformation event of phlogopite peridotite, before more recent faulting.

The age of these metasomatic events coincided in time with a period of extensional tectonics in the southern Alps (Bertotti, 1991), which implies a passive uplift of the subcontinental mantle. We envisage that during this uplift partial melts developed in a previously metasomatically enriched mantle. These melts rich in fluids and incompatible elements did not rise very far. Instead, they reacted with and modified the surrounding mantle peridotite.

ACKNOWLEDGEMENTS

This work was completed while the first author was at Dipartimento di Scienze della Terra, Università degli Studi di Milano, as recipient of a Post-Doctoral Research Fellowship. The research was partially supported by NSF grant EAR9316129 to E.A.M. and a grant from CNR (Centro Nazionale delle Ricerche). The mineral analyses were carried out with the assistance of D. Biondelli (electron microprobe) and N. Shimizu (ion microprobe). We thank B. Ferretti, V. Soi and A. Galletti for their help during field-work, and A. Tunesi for her cartographic support and constructive criticism.

REFERENCES

Anders, E. & Grevesse, N. (1989). Abundances of the elements: meteoritic and solar. *Geochimica et Cosmochimica Acta* **53**, 197–214.

Augè, T. (1987). Chromite deposits in the northern Oman ophiolite: mineralogical constraints. *Mineralium Deposita* **22**, 1–10.

Bertotti, G. (1991). Early Mesozoic extension and alpine shortening in the western Southern Alps: the geology of the area between Lugano

and Menaggio (Lombardy, northern Italy). Padova. *Memorie di Scienze Geologiche* **43**, 17–123.

Coltorti, M. & Siena, F. (1984). Mantle tectonite and fractionate peridotite at Finero (Italian Western Alps). *Neues Jahrbuch für Mineralogie, Abhandlungen* **149**, 225–244.

Cumming, G. L., Köppel, V. & Ferrario, A. (1987). A lead isotope study of the northeastern Ivrea Zone and the adjoining Ceneri Zone (N-Italy): evidence for a contaminated subcontinental mantle. *Contributions to Mineralogy and Petrology* **97**, 19–30.

Ferrario, A. & Garuti, G. (1990). Platinum-group minerals inclusions in chromitites of the Finero mafic–ultramafic complex (Ivrea-Zone, Italy). *Mineralogy and Petrology* **41**, 125–143.

Forbes, W. C., Mottana, A. & Morten, L. (1978). Gigantic mineral patches in the ultramafic rocks of the Finero Complex (Central Alps). *Proceedings of the 2nd Symposium, Ivrea–Verbano. Memorie della Società Geologica Italiana* **33**, 127–133.

Friedenreich, O. (1956). Die Chrom–Nickelverzungen des Peridotit-Stockes von Finero–Centovalli. *Schweizerische Mineralogische und Petrographische Mitteilungen* **36**, 228–243.

Grieco, G. (1998*a*). Le mineralizzazioni a cromite e PGE del complesso di Finero: relazioni con i processi metasomatici. Ph.D. thesis, University of Milan, 152 pp.

Grieco, G. (1998*b*). Chromite and PGE mineralizations of the Finero complex (southern Alps, Italy): relations with metasomatic processes. *Plinius* **19**, 134–140.

Hartmann, G. & Wedepohl, K. H. (1993). The composition of peridotite tectonites from the Ivrea Complex, northern Italy: residues from melt extraction. *Geochimica et Cosmochimica Acta* **57**, 1761–1782.

Hunziker, J. (1974). Rb–Sr and K–Ar age determination and the alpine tectonic history of the western Alps. *Memorie degli Istituti di Geologia e Mineralogia dell'Università di Padova* **31**, 1–54.

Irving, A. J. & Frey, F. A. (1984). Trace elements abundances in megacrysts and their host basalts: constraints on partition coefficients and megacryst genensis. *Geochimica et Cosmochimica Acta* **48**, 1201–1221.

Jaques, A. L. & Green, D. H. (1980). Anhydrous melting of peridotite at 0–15 Kb pressure and the genesis of tholeiitic basalts. *Contributions to Mineralogy and Petrology* **73**, 287–310.

Kelemen, P. B. (1990*a*). Reaction between ultramafic rock and fractionating basaltic magma I. Phase relations, the origin of the calc-alkaline magma series, and the formation of discordant dunite. *Journal of Petrology* **31**, 51–98.

Kelemen, P. B. (1990*b*). Reaction between ultramafic rock and fractionating basaltic magma II. Experimental investigation of reaction between olivine tholeiite and harzburgite at 1150–1050°C and 5 kb. *Journal of Petrology* **31**, 99–134.

Kelemen, P. B., Dick, H. J. B. & Quick, J. E. (1992). Formation of harzburgite by pervasive melt/rock reaction in the upper mantle. *Nature* **358**, 635–641.

Kushiro, I. (1969). The system forsterite–diopside–silica with and without water at high pressure. *American Journal of Science* **267A**, 269–294.

Kushiro, I. (1972). Effect of water on the composition of magmas formed at high pressures. *Journal of Petrology* **13**, 311–334.

Leblanc, M. & Ceuleneer, G. (1992). Chromite crystallisation in multicellular magma flow: evidence from a chromitite dike in the Oman ophiolite. *Lithos* **27**, 231–257.

Leblanc, M. & Nicolas, A. (1992). Ophiolitic chromitites. *Chronique de la Recherche Minière* **507**, 3–25.

Lu, M., Hoffmann, A. W., Mazzucchelli, M. & Rivalenti, G. (1997*a*). The mafic–ultramafic complex near Finero (Ivrea–Verbano Zone), I. Chemistry of MORB-like magmas. *Chemical Geology* **140**, 207–222.

Lu, M., Hoffmann, A. W., Mazzucchelli, M. & Rivalenti, G. (1997*b*). The mafic–ultramafic complex near Finero (Ivrea–Verbano Zone), II. Geochronology and isotope geochemistry. *Chemical Geology* **140**, 223–235.

Melcher, F., Grum, W., Simon, G., Thalhammer, T. V. & Stumpfl, E. F. (1997). Petrogenesis of the ophiolitic giant chromite deposits of Kempirsai, Kazakhstan: a study of solid and fluid inclusions in chromite. *Journal of Petrology* **38**, 1419–1458.

Neal, C. R. (1988). The origin and composition of metasomatic fluids and amphiboles, Bushveld Complex. *Contributions to Mineralogy and Petrology* **107**, 293–309.

Nicholson, D. M. & Mathez, E. A. (1991). Petrogenesis of the Merensky Reef in the Rustenburg section of the Bushveld Complex. *Contributions to Mineralogy and Petrology* **107**, 293–309.

Oppizzi, P. & Schaltegger, U. (1999). Zircon bearing plagioclasites from the Finero complex (Ivrea Zone): dating a late Triassic mantle. *Schweizerische Mineralogische und Petrographische Mitteilungen* **79**, 330–331.

Roggiani, A. G. (1948). *Ferro, Cromo e Platino nelle Rocce Basiche ed Ultrabasiche del Monte Gridone (Valle Vigezzo)*. Domodossola: Risveglio Ossolano.

Saager, R., Meyer, M. & Muff, R. (1982). Gold distribution in supracrustal rocks from Archean Greenstone Belts of the Southern Africa and from Paleozoic Ultramafic Complexes of the European Alps. Metallogenic and geochemical implications. *Economic Geology* **77**, 1–24.

Stähle, V., Frenzel, G., Kober, B., Michard, A., Puchelt, H. & Schneider, W. (1990). Zircon syenite pegmatites in the Finero peridotite (Ivrea zone): evidence for a syenite from a mantle source. *Earth and Planetary Science Letters* **101**, 196–205.

Vavra, G. & Schaltegger, U. (1999). Post-granulite facies monazite growth and rejuvenation during Permian to Lower Jurassic thermal and fluid events in the Ivrea zone (Southern Alps). *Contributions to Mineralogy and Petrology* **134**, 405–414.

Vavra, G., Gebauer, D., Schmid, R. & Compston, W. (1996). Multiple zircon growth and recrystallisation during polyphase Late Carboniferous to Triassic metamorphism in granulites of the Ivrea Zone (Southern Alps): an ion microprobe (SHRIMP) study. *Contributions to Mineralogy and Petrology***124**, 337–358.

Von Quadt, A. (1997). U–Pb zircon and Sr–Nd–Pb whole rock investigations from the continental deep drilling (KTB). *Geologische Rundschau* **86**, 258–271.

Voshage, H., Hunziker, J. C., Hofmann, A. W. & Zingg, A. (1987). A Nd and Sr isotopic study of the Ivrea Zone, Southern Alps, N-Italy. *Contributions to Mineralogy and Petrology* **97**, 31–42.

Zanetti, A., Mazzucchelli, M., Rivalenti, G. & Vannucci, R. (1999). The Finero phlogopite-peridotite massif: an example of subduction-related metasomatism. *Contributions to Mineralogy and Petrology* **134**, 107–122.

Zhou, M. F. & Robinson, P. T. (1997). Origin and tectonic environment of podiform chromite deposits. *Economic Geology* **92**, 259–262.

Zhou, M. F., Robinson, P. T. & Bai, W. J. (1994). Formation of podiform chromitites by melt/rock interaction in the upper mantle. *Mineralium Deposita* **29**, 98–101.